INSTITUTE OF PHYSICS PUBLISHING MEASUREMENT SCIENCE AND TECHNOLOGY

Meas. Sci. Technol. **17** (2006) 373–378 doi:10.1088/0957-0233/17/2/019

Fibre image techniques in digital stereomicroscopy

Kuang-Chao Fan[1,2], Ruijun Li[1] and Hsin-Ming Song[2]

[1] School of Instrumentation, Hefei University of Technology, Anhui, People's Republic of China
[2] Department of Mechanical Engineering, National Taiwan University, Taipei, Taiwan

E-mail: fan@ntu.edu.tw

Received 10 March 2005, in final form 16 November 2005
Published 4 January 2006
Online at stacks.iop.org/MST/17/373

Abstract
On the basis of the principles of structured light projection, phase shifting and triangulation, a new digital stereomicroscope system for micro-3D measurement is presented in this paper. Because the image fibre has many advantages such as direction changing and long distance transmitting without extra optics, this system also adopts it to project the structured light instead of the fixed optical systems. Thus, the measurement head is very small; the measurement distance and orientation could be changed expediently. Experiments showed that this is a useful system to measure the 3D profile of meso- and micro-scaled parts.

Keywords: micro-3D profile, fibre image, stereomicroscopy, phase shifting

(Some figures in this article are in colour only in the electronic version)

1. Introduction

Microscope has been a widely used tool for 2D visual inspection in science, industry and medicine. In many applications, however, the 2D inspection is no longer sufficient to meet the needs. The determination of three-dimensional (3D) topography of the specimen is a task that is becoming more and more important.

The technology of 3D topography was started by the projection moiré method [1]. Recently, many different measuring set-ups of stereomicroscopy based on structured light projection and triangulation principle for 3D topographic measurements have been carried out. Windecker *et al* [2], Wu [3] and Chang [4] used physical gratings and a phase shift mechanism to project the structured light patterns onto the object surface, and then captured the deformed pattern with a CCD camera. Zhang *et al* [5] and Huang *et al* [6] created computer generated patterns and their phase shifts, and then projected the patterns onto the surface through commercial digital light processing (DLP). Their measurement results are all satisfactory. But most of them are modified from the conventional visual stereomicroscopes. There are some drawbacks in this kind of system: (1) the specimen has to be preprocessed and fixed on the sample stage, (2) the stereoscopic angle is limited to the range of 10 to 20° between the project axis and the viewing axis depending on the stereomicroscope in use and (3) the field of view (FOV) is limited by the microscope's objective lens. Song [7] developed an independent stereomicroscope system composed of a PC to generate fringe patterns and analyse the deformed patterns, a DLP to project the patterns, an optical lens system to guide the light, a stand to mount the lens, an XY stage to place the sample and a zooming CCD camera to capture the image. Because of the adjustable angle of the CCD and the selectable lens system, the above-mentioned drawbacks (2) and (3) can be overcome.

In this paper we present an advanced version of Song's stereomicroscope that includes an image fibre bundle to direct the projecting patterns to any required angle via a developed miniature probe head. This is based on the concept of 'instrument fits the objects' rather than 'sample pieces fit the instrument'. This set-up not only extends the range of possible applications enormously but also makes the measurement more flexible. The principles and the set-up of our digital stereomicroscope system are introduced in section 2. Section 3 describes the data acquisition procedures, including the processes and principles of phase shifting and triangulation. Section 4 presents the data processing procedures, including phase unwrapping and image filtering. The system calibration

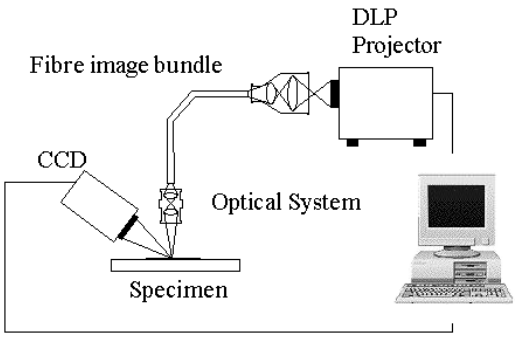

Figure 1. Schematic diagram of a fibre image transmitted stereomicroscope.

and some practical applications are given in section 5. Finally, section 6 summarizes the conclusions and discussions.

2. The principles of the system

2.1. Optical configuration and set-up

A new stereomicroscopy configuration utilizing an image fibre bundle to direct the projecting patterns to any required angle via a developed miniature probe head is proposed to combine the fringe pattern projection technique with the specially designed optical system and the probe head. The schematic diagram of the system is depicted in figure 1. The PC can generate black and white periodical sine patterns. Projected out through the DLP, the patterns enter the image fibre bundle through a directly coupled optical system. The single mode image fibre bundle can then transmit the patterns to its output end and project onto the specimen through an objective lens system. The line pitch and the light intensity can be adjusted by software according to the surface properties of the specimen. The fringes will be distorted by the topography of the specimen, and this image can be captured by a CCD. The phase shifting technique is also applied for the 3D reconstruction and a better resolution.

2.2. The optical modules

Three optical modules are employed in this system: two at both ends of the image fibre bundle and the third one is equipped to the CCD camera. In order to enhance the measurement precision, all optical modules are designed by telecentricity. There are at least three benefits [8].

(1) It provides nearly constant magnification over a range of working distances, virtually eliminating perspective angle error. This means that object movement does not affect image magnification. The assembly of our system, therefore, becomes more convenient.
(2) In a system with object space telecentricity, movement of the object towards or away from the lens will not result in the image getting bigger or smaller, and an object which has depth or extent along the optical axis will not appear as if it is tilted.
(3) In systems with image space telecentricity, image plane movements to focus or intentionally defocus the system will not change the image size.

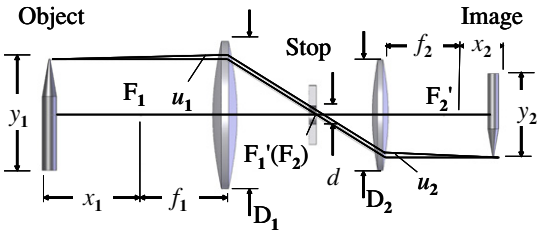

Figure 2. Configuration of one optical system, f: focal length, x: distance to focus, u: tilted angle of stop, D: diameter of the objective lens and d: diameter of the stop.

For clarity of expression, we assign the optical system connecting the DLP output and the fibre image bundle input as optical system 1, the one between the fibre output and the object as optical system 2 and the one between the object and the CCD input as optical system 3. The design of each optical system is described as follows.

The optical system normally considers two stages. The first stage is the dimensional design to determine the FOV, the focusing range, the lens diameter and the numeric aperture (*NA*). The second stage is the system aberration design, such as the lens type and the lens material. The second stage can be assisted by a CAD tool, such as ZEMAX.

Figure 2 shows the configuration of one optical system, where y_1 and y_2 denote the object size and image size, respectively. From Newton's law, we have

$$\frac{f_1}{f_2} = \frac{y_1}{y_2} \tag{1}$$

$$\frac{x_2}{x_1} = \frac{f_2^2}{f_1^2}. \tag{2}$$

Since y_1 and y_2 are known, the values of f_1, f_2, x_1, x_2 can be determined by equations (1) and (2).

Any point of the object will form the radius of confusion disc (R) on the image plane. This radius R is composed of three sources: the radius of the Airy disc (R_1), the radius of the confusion disc due to the offset from the ideal image plane (R_2) and the radius of the confusion disc due to the system aberration (R_3). The magnitude of R is the convolution of R_1, R_2 and R_3, among which

$$R_1 = \frac{0.61 \cdot \lambda}{n_2 \cdot \sin u_2} \qquad \text{and} \qquad R_2 = \frac{\Delta_2}{2} \cdot \tan u_2,$$

where λ is the wavelength of the light and Δ_2 is the depth of focus of the objective lens of the image. Suppose that the resolution of the CCD (pixel space) is c. In order to match the optical resolution to the CCD resolution, considering that after CCD calibration R_3 can be neglected, we let $R_1 + R_2 = c$.

$$\frac{0.61 \cdot \lambda}{n_2 \cdot \sin u_2} + \frac{\Delta_2}{2} \cdot \tan u_2 = c. \tag{3}$$

Since the angle of u_2 is small, we can assume $\sin u_2 \approx \tan u_2$. We can solve $\sin u_2$ from equation (3) and then solve the numerical aperture from $NA' = n_2 \cdot \sin u_2$. Moreover, according to the Lach invariant formula $y_1 \cdot f_1 \cdot \tan u_1 = -y_2 \cdot f_2 \cdot \tan u_2$, we can find *NA* of the objective lens from $NA = n_1 \cdot \sin u_1 \approx n_1 \cdot \tan u_1$. Consequently, we can find d, D_1 and D_2 from the following equations:

Table 1. Parameters of optical system 1 (unit: mm).

Focal length (object/image)	*NA* (object/image)	Resolution (LP mm^{-1}) (object/image)	Object FOV	Image FOV	x_1+f_1	x_2+f_2
54.4/13.2	0.015/0.06	120	ϕ25	ϕ6	75	18

Table 2. Parameters of optical system 2 (unit: mm).

Focal length (object/image)	*NA* (object/image)	Resolution (LP mm^{-1}) (object/image)	Object FOV	Image FOV	x_1+f_1	x_2+f_2
36.9/12.8	0.06/0.04	120	ϕ6	ϕ8	18	25

Table 3. Parameters of optical system 3 (unit: mm).

Focal length (object/image)	*NA* (object/image)	Resolution (LP mm^{-1}) (object/image)	Object FOV	Image FOV	x_1+f_1	x_2+f_2
17.6/13.2	0.04/0.06	120	ϕ8	ϕ6	56	17

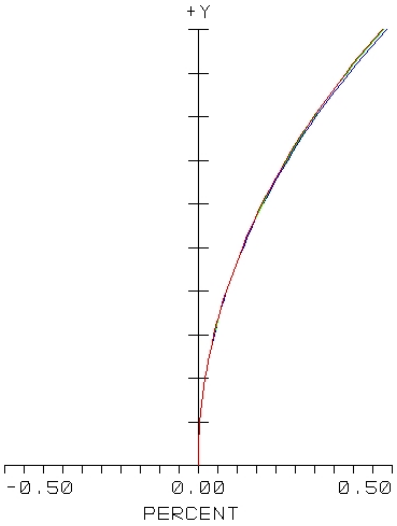

Figure 3. Image distortion curve along the radius direction of optical system 2.

$$d = 2f_1 \cdot \tan u_1 = 2f_2 \cdot \tan u_2$$
$$D_1 = y_1 + 2f_1 \cdot \tan u_1$$
$$D_2 = y_2 + 2f_2 \cdot \tan u_2.$$

Once all parameters f_1, f_2, x_1, x_2, d, D_1, D_2, NA and NA' are determined, we can process the optimum light trace with the ZEMAX software.

According to the above analysis, tables 1 to 3 summarize the relevant parameters of optical systems 1 to 3. Figure 3 plots the image distortion curve along the radius direction of optical system 2. It is seen that the maximum distortion is below 0.5% and the diameter of the dispersion disc at the marginal point of the FOV is less than 10 μm.

2.3. The probe head design and the system set-up

In order to be flexible in practical use, a small and compact optical head was designed to include the fibre bundle end, optical system 2, optical system 3 and the CCD, as illustrated in figure 4. The reflection angle is 45°. The CCD is a 1/2-inch chip with 1280 × 1024 pixels. The end dimensions of the head are 24 mm × 55 mm.

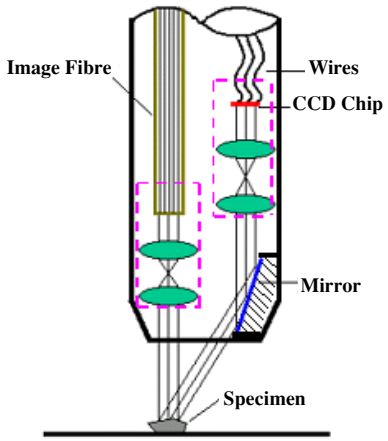

Figure 4. The probe head.

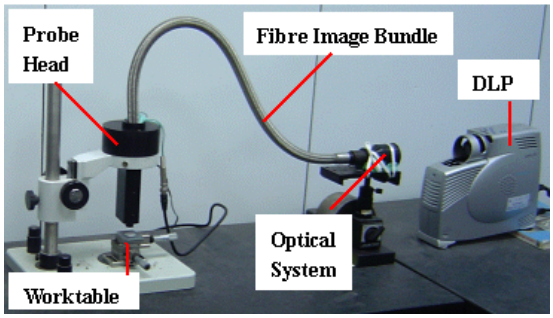

Figure 5. The system setup.

The experimental set-up is shown in figure 5. We used a 600 × 800 DLP to project sine wave patterns. The grey level and the number of lines could be computer controlled. A compound glass image fibre bundle with 80 000 pixels was used to transmit the projected image. The diameter of a single fibre is 15 μm, *NA* is 0.55, spectrum range is 380–1300 nm, and attenuation and resolution are 300–600 dB km^{-1}

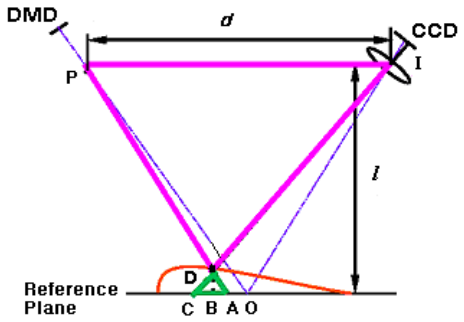

Figure 6. Triangulation principle.

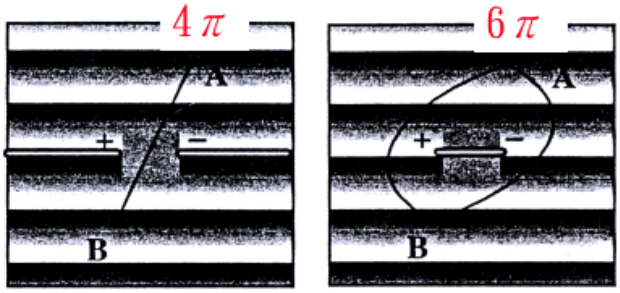

(*a*) (*b*)

Figure 7. The branch cut algorithm: (*a*) straight line phase unwrapping and (*b*) branch cut line phase unwrapping.

Figure 8. Original image with grid pattern.

and 36 LP mm^{-1}, respectively. All the optical systems were designed by telecentric lenses. The measurement range is about 4.5 mm (L) × 3.6 mm (W) × 3.5 mm (H). The achievable resolution of the projected pattern is equal to the resolution of the optical system, which is 120 LP mm^{-1}. Vertical resolution is, therefore, 8.3 μm. The stand-off distance of the probe head is about 45 mm. Any object to be measured can be placed on the worktable, or the probe head can be freely moved to the front of the object at the stand-off distance.

3. Measurement principle

The 3D shape reconstruction is based on the triangulation principle [9] and assisted by the phase shifting technique [5, 10, 11].

As shown in figure 6, the geometrical relationship among the structured light emitting point (P), the CCD lens centre (l) and the point of projection on the object surface (D) forms up a triangulation. Without the object the DMD centre shall project onto the reference plane at point O, and any point of the pattern shall project onto the reference plane at an offset position, say point A. Due to the surface height BD, point A will shift to point C on the image plane. The difference in phases of points A and C on the image plane can be expressed by $\phi_{AC} = \phi_C - \phi_A$. From the triangulation principle we can obtain equation (4). Distances l and d are known during the system set-up. The constant K can be obtained by the calibration of gauge blocks:

$$\overline{DB} = \frac{l}{d}\overline{AC} = K\phi_{AC} = K(\phi_C - \phi_A) \tag{4}$$

The triangulation method only solves the surface heights corresponding to the pattern line centres. In order to increase the measurement resolution of any point between two adjacent lines, we have to know its corresponding phase so as to convert its relative proportional height. Phase shifting of the sinusoidal pattern is an effective solution. This research adopts four-phase shift method [11] in which the phase can be evaluated as $\phi = \tan^{-1}\left[\frac{I_4 - I_2}{I_1 - I_3}\right]$ using four different intensity patterns I1, I2, I3 and I4.

This study adopts the noise-immune phase unwrapping algorithm, called the branch cut algorithm, developed by Goldstein [12]. As shown in figure 7, a shadow image is located along the connecting route between points Aand B. The calculated phase change will be 4π (figure 7(a)), which is wrong in comparison with the true phase change of 6π. The branch cut algorithm will automatically generate a shortest detoured path if any discontinuous image blocks the phase connecting route. The unwrapped phase will thus be corrected to the true value of 6π (figure 7(b)).

4. Image filtering

Because light cannot pass through the cladding of the single fibre, many hexagonal grids will appear in the captured image. The fewer the number of fibres in the bundle, the more obviously these grids can be seen. Figure 8 shows an example of the captured image transmitted by an image fibre bundle with only 13 000 fibres. These grids have a great effect on the subsequent work, such as image processing, phase wrapping, 3D coordinate calculation and so on. How to reduce the grids efficiently is, therefore, crucial to the whole system. Generally speaking, two methods can be adopted for this problem. One is to select a fibre bundle containing more fibres while keeping the image size constant; the other is to apply an image-processing technique. Although we have selected the fibre bundle with 80 000 fibres in our developed system, the grid phenomenon could be reduced to a certain degree; we still applied the image processing technique to remove the remaining noise. This study adopted the image smoothing algorithm by the Butterworth low pass filter [13]. The hexagonal grids can be considered as high frequency signals compared to the larger fringe line spacing. Therefore, applying the low pass filtering technique can effectively remove the hexagonal grids. Figure 9 demonstrates the effect of grid removal from the image of

Figure 9. Filtered image.

figure 8. Although the low pass filter, by its nature, will blur the filtered image, it will not affect the phase unwrapping calculation in practice.

5. Experimental results and discussion

5.1. System calibration

A grade 0 gauge block of 1200 μm was adopted as a reference height. The projected pattern was operated by (1) phase shifting, (2) phase unwrapping and (3) triangulation algorithms in sequence. The obtained phase constant K was 36.4572 μm deg^{-1}. Using this constant, a second gauge block of 1300 μm was tested and the calculated phase difference between the base plate and the upper surface was 35.9225°. Substituting the calibrated constant K into equation (4), the measured height was 1309.6 μm. This process was repeated seven times. The averaged value was 1310 μm (accuracy of about 0.8% FS) and the standard deviation was 4.5 μm.

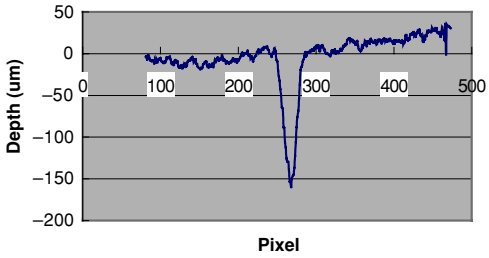

Figure 11. Measured profile of a V-groove.

5.2. Applications

In the first application, we took a micro V-groove to measure. This V-groove, made by the MEMS process, is used for supporting the optical fibre. Figures 10(*a*)–(*d*) are the distorted images whose phases are 0°, 90°, 180° and 270°, respectively. Four-step phase shifting arithmetic was used to reconstruct the 3D contour. Figures 10(*e*) and (*f*) are the wrapped and unwrapped images, respectively. Figure 10(*g*) plots the reconstructed 3D contour. The nominal depth of 155 μm was measured by a 2.5D digital profile projector. We measured ten times with our system. The average value was 161.7 μm with an average error of about 1.08% and standard deviation 1.73 μm. One typical result is shown in figure 11.

The second case was to measure the character of a Chinese coin. The character is about 4 mm × 3 mm in surface area and 0.3 mm in height. Figure 12 shows the measured images and the 3D contour.

The third case was to measure a small steel sphere of nominal diameter 3.2 mm. Figure 13(*a*) shows the captured image pattern. The reconstructed 3D profile is plotted in figure 13(*b*). The measured diameter is about 3.25 mm. Since the lower part of the sphere is in shadow, only the top profile is obtainable.

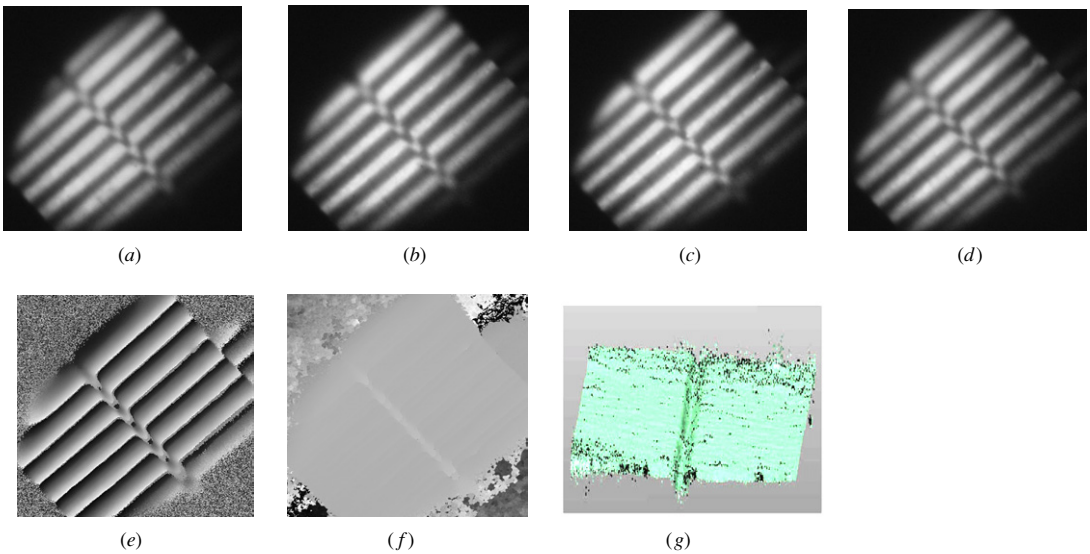

Figure 10. Measurement of a V-groove: (*a*) 0° image, (*b*) 90° image, (*c*) 180° image, (*d*) 270° image, (*e*) wrapped image, (*f*) unwrapped image and (*g*) 3D reconstruction.

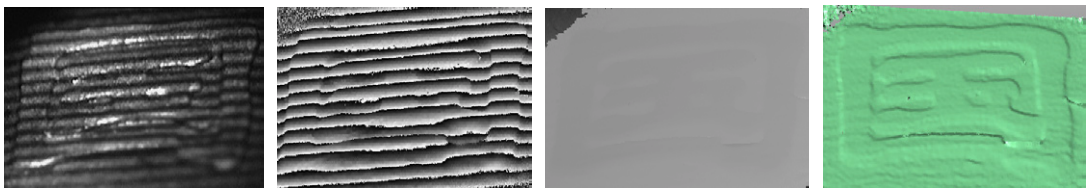

(*a*) (*b*) (*c*) (*d*)

Figure 12. Measured results of a character of a Chinese coin: (*a*) image pattern, (*b*) wrapped image, (*c*) unwrapped image and (*d*) 3D contour.

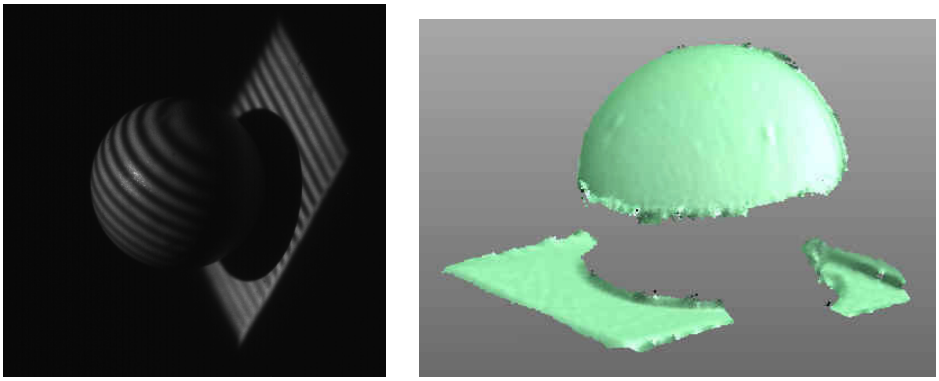

(*a*) (*b*)

Figure 13. Measurement of a small ball: (*a*) captured image and (*b*) reconstructed profile.

6. Conclusions

A new digital stereomicroscope system based on the fibre image technique is presented in this paper. Such a system overcomes the disadvantages of common stereomicroscopes in terms of extendable length and flexible orientation. It also realizes the concept of 'fitting the instrument to the object'. For any localized tiny portion of a large object, this system can easily move the optical head to the required position and take its 3D profile measurement. Through the design of telecentric lens systems, the measuring range can reach to 4.5 mm (L) × 3.6 mm (W) × 3.5 mm (H) within which the profile change will not alter the image size. The current system accuracy is about 0.8% of the measured full scale.

Acknowledgments

The work reported forms part of a research programme funded by the Tjing Ling Industrial Research Institute of National Taiwan University and the Natural Science Foundation of China (50275048).

References

[1] Takasaki H 1970 Moiré topography *Appl. Opt.* **9** 1467–72

[2] Windecker R, Fleischer M and Tiziani H J 1997 Three-dimensional topometry with stereomicroscopes *Opt. Eng.* **36** 3372–7

[3] Wu S D and Lu G W 2000 Optical phase shift triangulation technique (PST) for noncontact surface profiling *US Patent no* 6040910

[4] Chang M and Lin K H 2001 Noncontact probe for profilometric measurement of small-form parts *Opt. Eng.* **40** 2057–8

[5] Zhang C P, Huang P S and Chiang F P 2001 High-speed phase shifting profilometry *Proc. SPIE* **4189** 122–8

[6] Huang H S, Hu Q Y, Jin F and Chiang F P 1999 Color-encoded digital fringe projection technique for high-speed three-dimensional surface contouring *Opt. Eng.* **38** 1065–71

[7] Song H M 2004 Development of a stereomicroscope *Master Thesis* National Taiwan University

[8] Michalski J 2005 What is telecentricity *Technical Article* Edmund Optics Co. http://www.edmundoptics.com.sg

[9] Fan K C and Tsai T H 2001 Optimum shape error analysis of the matching image for a free-form surface *Robot. Comput.-aided Manuf.* **17** 215–22

[10] Creath K 1988 Phase-measurement interferometry techniques *J. Prog. Opt.* **16** 351–93

[11] Creath K and Schmit J 1996 *N*-point spatial phase-measurement techniques for non-destructive testing *Opt. Lasers Eng.* **24** 365–79

[12] Goldstein R M, Zebker H A and Werner C L 1988 Satellite radar interferometry: two-dimensional phase unwrapping *J. Radio Sci.* **23** 713–20

[13] Gonzalez R C and Wintz P 1977 *Digital Image Processing* (Reading, MA: Addison-Wesley)